West Nile virus-inclusive single-cell RNA sequencing reveals heterogeneity in the type I interferon response within single cells

Justin T. O'Neal[a,b], Amit A. Upadhyay[b,d], Amber Wolabaugh[b,d], Nirav B. Patel[c], Steven E. Bosinger[b,c,d], Mehul S. Suthar[a,b]#*

[a]Department of Pediatrics, Division of Infectious Disease, Emory University School of Medicine, Atlanta, Georgia, USA

[b]Emory Vaccine Center, Yerkes National Primate Research Center, Atlanta, Georgia, USA

[c]Yerkes Genomics Core, Yerkes National Primate Research Center, Atlanta, Georgia, USA

[d]Department of Pathology and Lab Medicine, Emory University School of Medicine, Atlanta, Georgia, USA

Running Head: West Nile virus-inclusive single-cell RNA sequencing

#Address correspondence to Mehul S. Suthar, mehul.s.suthar@emory.edu.

*Present address: Yerkes National Primate Research Center, Atlanta, Georgia, USA.

Abstract: 232 words; Importance: 122 words; and Text: 4,850 words.

ABSTRACT

West Nile virus (WNV) is a neurotropic mosquito-borne flavivirus of global importance. Neuroinvasive WNV infection results in encephalitis and can lead to prolonged neurological impairment or death. Type I interferon (IFN-I) is crucial for promoting antiviral defenses through the induction of antiviral effectors, which function to restrict viral replication and spread. However, our understanding of the antiviral response to WNV infection is mostly derived from analysis of bulk cell populations. It is becoming increasingly apparent that substantial heterogeneity in cellular processes exists among individual cells, even within a seemingly homogenous cell population. Here, we present WNV-inclusive single-cell RNA sequencing (scRNA-seq), an approach to examine the transcriptional variation and viral RNA burden across single cells. We observed that only a few cells within the bulk population displayed robust transcription of IFN-β mRNA, and this did not appear to depend on viral RNA abundance within the same cell. Furthermore, we observed considerable transcriptional heterogeneity in the IFN-I response, with genes displaying high unimodal and bimodal expression patterns. Broadly, IFN-stimulated genes negatively correlated with viral RNA abundance, corresponding with a precipitous decline in expression in cells with high viral RNA levels. Altogether, we demonstrated the feasibility and utility of WNV-inclusive scRNA-seq as a high-throughput technique for single-cell transcriptomics and WNV RNA detection. This approach can be implemented in other models to provide insights into the cellular features of protective immunity and identify novel therapeutic targets.

IMPORTANCE

West Nile virus (WNV) is a clinically relevant pathogen responsible for recurrent epidemics of neuroinvasive disease. Type I interferon is essential for promoting an antiviral response against WNV infection; however, it is unclear how heterogeneity in the antiviral response at the single-cell level impacts viral control. Specifically, conventional approaches lack the ability to distinguish differences across cells with varying viral abundance. The significance of our research is to demonstrate a new technique for studying WNV infection at the single-cell level. We discovered extensive variation in antiviral gene expression and viral abundance across cells. This protocol can be applied to primary cells or *in vivo* models to better understand the underlying cellular heterogeneity following WNV infection for the development of targeted therapeutic strategies.

INTRODUCTION

Mosquito-borne flaviviruses represent a significant public health burden, annually accounting for millions of infections worldwide that, in certain cases, can culminate in severe systemic or neuropathological outcomes (1-4). West Nile virus (WNV), a member of the *Flaviviridae* family, causes yearly epidemics of encephalitis and virus-induced myelitis on a global scale with nearly 50,000 reported cases of WNV disease and over 21,000 cases of neuroinvasive disease from 1999 to 2016 in the United States alone (1-4). Currently, there are no licensed vaccines or approved targeted therapeutics to prevent or treat WNV-infected patients, underscoring the need to better understand the cellular response to WNV infection (1-4).

Type I IFN (IFN-α/β or IFN-I) is the first line of defense against viral infection and coordinates the early antiviral programs to restrict viral replication, as well as shape the adaptive immune response (5-14). Loss of IFN-I signaling in WNV-infected mice results in uncontrolled viral replication and rapid mortality, demonstrating that the IFN-I response is required for protective immunity (9, 11, 14, 15). Pattern recognition receptors, including toll-like receptors (TLRs) and retinoic acid-inducible gene I (RIG-I)-like receptors (RLRs), detect broad viral signatures, such as 5'-triphosphate ssRNA or dsRNA, in the cytosolic and endosomal compartments (9, 11, 12, 14). For flavivirus infection, RLRs are critical for inducing IFN-I and binding to cytosolic viral RNA signals through adaptor proteins, such as mitochondrial antiviral signaling protein (MAVS), to activate transcription factors and induce interferon regulatory factor (IRF)-mediated transcription of IFN-β (*Ifnb1*) and a subset of IFN-stimulated genes (ISGs) (9, 11, 12, 14, 16-22). Signaling in both an autocrine and paracrine manner, secreted IFN-β binds IFN-

I receptor (IFNAR1/2 heterodimer) to activate Janus kinases, Jak1 and Tyk2, which phosphorylate signal transducer and activator of transcription 1 (STAT1) and STAT2 (7, 9, 10, 12, 18-21, 23-27). Phosphorylated STAT1 and STAT2 form a heterodimer and recruit IRF9 to form the ISG factor 3 (ISGF3) complex. The ISGF3 complex then translocates to the nucleus and induces IFN-stimulated response element (ISRE)-regulated genes, thereby reshaping the cellular landscape to an antiviral state (5, 7, 9, 12, 18-21, 23-28).

The induction of IFN-I and ISGs within a bulk population of infected cells has been well characterized. However, mean values obtained via conventional bulk assays mask transcriptional differences between infected and bystander cells and obscure any heterogeneity present within the infected population. Recently, single-cell studies have examined the heterogeneity across virally infected cells. Findings with influenza virus, poliovirus, dengue virus (DENV) and Zika virus (ZIKV) have revealed extensive variation in viral RNA abundance within single cells (29-31). Using high dimensional mass cytometry by time-of-flight (CyTOF) analysis, others have described differences in IFN-induced and pro-inflammatory cytokine production in infected and bystander human dendritic cells following DENV infection (32). Studies examining IFN-I induction at the single-cell level have used fluorescently-tagged cells, single-mRNA molecule *in situ* hybridization, single-cell quantitative PCR (qPCR), and single-cell RNA sequencing (scRNA-seq) (16-19, 27, 33). Previous studies have found that only a small fraction of infected cells express *Ifnb1* mRNA (17-19, 27). This is thought to be attributable to stochasticity in signaling components and downstream signaling cascades leading to transcription factor activation or variability in the processes of *Ifnb1* expression, perhaps

107 at the level of chromatin organization (16-19, 34-36). Using PRR agonists or
108 nonproductive viral infection, others have demonstrated that IFN-I-dependent paracrine
109 signaling is pivotal in amplifying the host antiviral response (16-19, 26, 27). Lastly,
110 single-cell transcriptomic studies have also been used to globally investigate virus-host
111 interactions and identify novel candidate genes for host-targeted therapeutics (31).
112 Knockdown screens or knockout studies can only probe a subset of nonessential host
113 genes, limiting their scope (37-42). However, virus-inclusive scRNA-seq is a powerful
114 platform for the discovery of novel proviral and antiviral candidate genes in an unbiased
115 manner as recently highlighted by Zanini and colleagues with DENV and ZIKV (31).

116 Altogether, these studies have shed considerable light on the transcriptional
117 differences present in single cells, and specifically with *Ifnb1* expression and viral RNA
118 abundance. However, we still lack a thorough understanding of the cellular
119 heterogeneity in the IFN-I response following WNV infection. Population-level
120 transcriptional analyses are valuable and widely used approaches, but in certain cases
121 can belie gene expression patterns, such as bimodal variation, which can only be
122 observed at single-cell resolution (18, 27, 33). To better understand the underlying
123 transcriptional differences across cells with varying viral abundance, we developed
124 WNV-inclusive scRNA-seq, a modified SMART-Seq protocol that incorporates a virus-
125 specific primer for parallel recovery of host messenger RNA (mRNA) and viral RNA
126 from single cells. We found that only a small fraction of cells exhibited robust *Ifnb1*
127 expression, and this did not significantly correlate with high viral RNA. We observed
128 considerable transcriptional heterogeneity in ISG expression and viral RNA abundance
129 across cells. ISGs exhibited both unimodal and bimodal variation and were negatively

130 correlated with intracellular viral RNA, displaying a steep decline in gene expression
131 with increasing viral abundance. Combining single-cell mRNA sequencing with
132 quantification of non-polyadenylated viral RNA, we present WNV-inclusive scRNA-seq
133 as a high-throughput technique for single-cell transcriptome analysis of WNV-infected
134 cells.
135
136
137

RESULTS

Population-level analysis of WNV infection in murine fibroblast L929 cells. We first modeled WNV infection kinetics in murine fibroblast L929 cells, an IFN-competent cell line extensively used to study IFN-I-dependent signaling (19, 43). Cells were infected at a multiplicity of infection (MOI) of 0.1, 1 or 10, as determined on BHK-21 cells, and intracellular viral envelope (E) protein immunostaining was performed at 6, 12, 24 and 48 hr post-infection. Infected cells were labeled with WNV E16 antibody (Ab), which recognizes a domain III (DIII) neutralizing epitope within the E protein (44). For all three MOIs, nearly 100% of cells stained positive for intracellular viral E protein by 48 hr post-infection (Fig. 1A). At a MOI of 10, intracellular viral E protein was detected in nearly 100% of cells as early as 24 hr post-infection, suggesting that the majority of these cells were likely infected during primary virus adsorption (Fig. 1A). For cells infected at a MOI of 1, intracellular viral E protein was detected in approximately 60% of cells at 24 hr post-infection (Fig. 1A).

To diminish asynchronous second-round infection, cells were infected with WNV (MOI of 1) and incubated in the presence of WNV E16 neutralizing Ab. Inoculation with UV-inactivated WNV served as a non-replicating input control for internalized viral RNA, and no expression of viral E protein was detected (Fig. 1B, 1C). Notably, limiting *in vitro* spread resulted in a 5.5-fold decrease in the percentage of viral E protein-positive cells (10.6%) at 24 hr post-infection, corresponding with a comparable 5.2-fold reduction in viral RNA levels (Fig. 1B, 1C). Collectively, these two conditions, WNV and WNV (+Ab), provide a cell population with a range of viral abundance and another of predominantly

bystander cells with which to survey the IFN-I response at the population and single-cell level in all subsequent analyses.

Before pursuing a single-cell approach, we next sought to evaluate transcriptional changes following WNV infection at the population level by bulk RNA-seq. As expected, numerous genes associated with the innate immune response and antiviral defense response were up-regulated following infection (Fig. 1D, 1E). Furthermore, the majority of these genes were expressed at similar levels independent of reduced asynchronous second-round infection (Fig. 1D, 1E). ISGs and PRR genes exhibited a more consistent level of mean gene expression across these two conditions (Fig. 1E). Conversely, IFN-I and cytokine genes displayed the most variability in expression between genes within their respective categories (Fig. 1E). Most notably, *Ifna2* and *Ifna5* displayed around two-fold higher levels of expression when allowing for *in vitro* spread, although *Ifna2* dropped outside of the pre-selected significance cutoff ($p < 0.01$; Fig. 1E, 1F). This population-level analysis provides a contextual fundamental framework from which to build as we examine the transcriptional differences observed across single cells. Leveraging single-cell sequencing techniques complemented with viral RNA detection, we next extended the resolution of our analysis to single cells to better understand the underlying transcriptional heterogeneity present following WNV infection.

WNV-inclusive scRNA-seq captures mRNA and viral RNA from single cells. WNV-inclusive scRNA-seq is adapted from the well-established Smart-seq2 protocol (45) and the commercially available SMART-Seq v4 Ultra Low Input RNA Kit (Takara) used for

scRNA-seq. The SMART-Seq v4 protocol is modified to include a virus-specific primer (WNV SC primer) during the reverse transcription (RT) step. For scRNA-seq analysis, L929 cells are inoculated with virus for 1 hr at a MOI of 1 and then incubated in the presence or absence of WNV E16 neutralizing Ab (44) for 24 hr (Fig. 2A). Viable single cells are sorted by conventional flow cytometry into 96-well plates containing 10 µL lysis buffer per well (Fig. 2B). In the RT reaction, 3' SMART-Seq CDS Primer II A (30-nucleotide poly-dT sequence with a 5' 25-nucleotide ISPCR universal anchor sequence (45)) and WNV SC primer (21-nucleotide sequence complementary to positive-strand viral RNA with a 5' 25-nucleotide ISPCR universal anchor sequence (45)) are added to capture host transcripts and viral RNA, respectively (Fig. 2C). Following template switching, PCR Primer II A served as the primer for parallel downstream amplification of both host and viral complementary DNA (cDNA) (Fig. 2C). Samples underwent Nextera tagmentation and were sequenced on an Illumina HiSeq at a depth of approximately 1 million reads per cell (27, 46). Altogether, we successfully captured and profiled a total of 127 cells across three conditions: Mock, WNV, and WNV (+Ab). The outlined approach delivers exceptional coverage and sequencing depth allowing for accurate quantification of host transcripts and non-polyadenylated viral RNA.

Viral RNA was successfully recovered from single cells following WNV infection, and the majority of WNV reads were aligned with the targeted region of the WNV genome (Fig. 2D). To ensure that the addition of WNV SC primer did not adversely affect the recovery of host mRNAs, the concentration of WNV SC primer was carefully titrated and cDNA quality was evaluated on an Agilent 2100 Bioanalyzer (Supplementary Fig. 1). Furthermore, we examined the levels of housekeeping genes

(*Gapdh*, *Rpl5*, *Arf1* and *Pgk1*) across cells in all three conditions: Mock, WNV, and WNV (+Ab). Unsurprisingly, expression of housekeeping genes was not significantly different between mock and infected conditions, demonstrating that amplification of viral RNA does not impair recovery of host mRNA (Fig. 2E).

Heterogeneity in viral RNA abundance and ISG induction at single-cell resolution. At the single-cell level, we observed large differences in viral RNA abundance in the presence and absence of limited *in vitro* spread (Fig. 2D). In the absence of neutralizing antibody, we detected a wide range of intracellular viral RNA levels, with the majority of cells having greater than 2^{10} viral RNA counts per million transcripts (Fig. 2D). Interestingly, only 24% of cells had greater than 2^{10} viral RNA counts per million transcripts when limiting asynchronous secondary infection (Fig. 2D). Furthermore, the heterogeneity of viral RNA abundance in the presence of neutralizing antibody suggests that there is variability in WNV replication during the primary round of infection (Fig. 2D). Notably, the percentage of single cells positive for viral RNA (Fig. 2D) is significantly higher than the percentage predicted by flow cytometry-based viral E protein immunostaining for both infection conditions (Fig. 1B).

When examining transcriptional dynamics across single cells, we noticed some interesting trends. Only a small fraction of WNV-infected cells produced greater than 2^5 *Ifnb1* counts per million transcripts (Fig. 3A). Intriguingly, we observed a similar expression signature for *Ifna4* and *Ifna2* despite high levels of *Irf7*, a transcription factor that drives IFN-α production (47-49), in the majority of cells (Fig. 3A). Furthermore, we identified three chemokine genes (*Ccl5*, *Ccl4* and *Cxcl11*) that displayed comparable

cellular distributions to IFN-I genes. Other pro-inflammatory cytokine genes, *Cxcl10*, *Tnf*, *Il6* and *Il23a*, exhibited cellular heterogeneity but still maintained a portion of cells with no detectable transcript. Genes *Ddx58* and *Dhx58*, which respectively encode the RLRs RIG-I and LGP2 (Laboratory of Genetics and Physiology 2), were highly expressed with most cells containing greater than 2^5 counts per million transcripts (Fig. 3B). Interestingly, *Tlr3* and *Ifih1*, another important RLR gene that encodes MDA5 (melanoma differentiation-associated gene 5), displayed greater variation in expression across cells, including a fraction with no detectable transcript (Fig. 3B). Components of the ISGF3 complex (*Irf9*, *Stat1* and *Stat2*) are critical for IFN-I signaling and are induced to greater than 2^5 counts per million transcripts in the majority of cells (Fig. 3B). Next, we sought to examine the expression patterns for a panel of experimentally validated WNV-targeting antiviral effector genes (*Rsad2*, *Tnfsf10*, *Ifi44l*, *Oas1b*, *Oas3*, *Ifitm3*, *Eif2ak2* and *Mov10*) and two well-established ISGs (*Ifit3* and *Mx1*) (26, 42, 50-58). Antiviral effector genes feature both unimodal (*Tnfsf10*, *Ifi44l*, *Ifitm3*, *Eif2ak2*, *Mov10* and *Mx1*) and bimodal (*Rsad2*, *Oas1b*, *Oas3* and *Ifit3*) variation across single cells (Fig. 4). Notably, several genes (*Ddx58*, *Tlr3*, *Stat1*, *Tnfsf10*, *Eif2ak2*, *Ifit3* and *Mx1*) revealed significantly different transcriptional signatures across cells with and without limited *in vitro* spread (Fig. 3B, 4). Strikingly, most cells have no detectable reads for *Tnfsf10* and *Mx1* when allowing for *in vitro* spread; however, in the presence of neutralizing Ab, the inverse is true (Fig. 4).

Correlation between host gene expression and viral RNA abundance for single cells. Building upon our ability to assess viral RNA abundance in singe cells, we

252 calculated Spearman's correlation coefficients for host gene expression and viral RNA
253 burden across all WNV cells, which spanned a range of viral RNA levels. To
254 comprehensively identify pathways that might be linked to viral RNA abundance, we
255 performed gene ontology (GO) enrichment analysis using the online bioinformatics tool
256 DAVID (59, 60), wherein we independently evaluated all positively correlated ($\rho > 0.35$)
257 and negatively correlated ($\rho < -0.35$) genes of significance ($p < 0.001$). The top
258 pathways extracted from the GO enrichment analysis for negatively correlated genes
259 were the antiviral defense response, cellular response to IFN-β, response to virus,
260 negative regulation of viral replication, innate immune response and antigen processing
261 and presentation via MHC I (class I major histocompatibility complex molecule) (Fig.
262 5A). For the positively correlated gene set, the top pathways included transcriptional
263 regulation, amino acid transport, ribosomal RNA (rRNA) processing, regulation of
264 protein ubiquitination and ER stress response, providing a broad description of viral
265 RNA-correlated genes (Fig. 5A). Next using curated gene lists from published large-
266 scale ISG screen and single-cell transcriptomic studies (26, 61, 62), we examined the
267 distribution of correlation coefficients for ISGs and cell cycle-associated genes
268 subdivided by phase (G1/S, S, G2/M, M and M/G1). Predictably, the majority of genes
269 do not correlate with viral RNA abundance, and the distribution of coefficients skews
270 heavily towards zero (Fig. 5B). When assessing viral RNA correlations for cell cycle-
271 associated genes, most genes were not significantly positively or negatively correlated,
272 although minor shifts were observed for S, M and M/G1 phase genes (Fig. 5B).
273 Interestingly, 124 out of 294 ISGs were negatively correlated with viral RNA
274 corresponding with a dramatic shift in the coefficient distribution (Fig. 5B). As predicted

by the GO enrichment analysis, numerous genes associated with the ER stress response (*Gadd45a*, *Ppp1r15a*, *Selenos*, *Ddit3*, *Atf4* and others) were strongly positively correlated with viral abundance (Fig. 5B). A subset of correlated ISGs and panel of non-correlated cytokine genes are represented in a correlation matrix (Fig. 5C). Negatively correlated ISGs strongly clustered together with high correlation coefficients approaching 1 (Fig. 5C). Conversely, ISGs positively correlated with viral RNA only weakly correlated with other positively correlated ISGs (Fig. 5C). Many cells expressing high levels of IFN-I and pro-inflammatory cytokines also featured elevated viral abundance, but not to the extent of reaching significant positive correlation (Fig. 5C). Scatter plots were generated for a subset of viral RNA-correlated genes and collated in order of increasing correlation coefficients (Fig. 6). Trends associated with negatively correlated ISGs mostly featured a precipitous decline in gene expression as viral RNA levels in single cells exceeded around 2^{15} counts per million transcripts (Fig. 6). Alternatively, positively correlated genes often were characterized by slopes near or less than 1 (Fig. 6). For WNV-validated antiviral effector genes (*Rsad2*, *Tnfsf10*, *Ifi44l*, *Oas1b*, *Oas3*, *Ifitm3*, *Eif2ak2* and *Mov10*), all genes are negatively correlated with viral RNA as expected (Fig. 6). Interestingly, *Tnfsf10*, *Ifi44l* and *Mx1* present unique correlation trends with viral RNA in that the cells with the highest viral abundance have no detectable transcripts for these genes (Fig. 6).

DISCUSSION

Standard scRNA-seq protocols with oligo-dT-based priming have been used to examine transcriptional dynamics during viral infection, but the unique genomic structure of flaviviruses, and other non-polyadenylated viruses that are clinically important pathogens, represents a distinct hurdle for such studies (29). We have independently developed and demonstrated the feasibility of WNV-inclusive scRNA-seq as an attractive approach for the quantification of host transcripts and viral RNA within single cells. This protocol, in combination with previously published work by Zanini and colleagues (31), establishes virus-inclusive scRNA-seq as a viable and tractable system for other non-polyadenylated RNA viruses.

WNV-inclusive scRNA-seq revealed extensive transcriptional heterogeneity in viral RNA abundance and the IFN-I response across single cells (Fig. 2D, 3, 4). The majority of WNV reads mapped to the targeted region of the WNV genome (Fig. 2D). However, minimal non-random background was observed in Mock cells with a median value of 45 WNV CPM for Mock cells, as compared to 37246 WNV CPM for WNV cells. This background may result from index hopping (63), and could be accounted for in subsequent iterations by using unique indexes. In support of published findings (17-19, 27), we found that few cells produce IFN-β transcript following viral infection (Fig. 3A). However, we observed a strong induction of numerous ISGs (*Irf7*, *Ddx58*, *Dhx58*, *Irf9*, *Stat1* and *Stat2*) with high unimodal expression signatures (Fig. 3), highlighting the well-established importance of IFN-I-dependent paracrine signaling (16-19, 26, 27). Interestingly, we saw a bifurcation in ISG correlations with viral RNA, wherein 124 out of 294 ISGs were negatively correlated with intracellular viral abundance (Fig. 5B).

Furthermore, a considerable fraction of ISGs featured a precipitous downward trend in expression with increasing viral RNA, dissimilar to the gradual upward trend exhibited by positively correlated genes (Fig. 6). Collectively, these findings are reflective of the dynamic balance and interplay between host and viral factors within a single cell. This represents the first single-cell transcriptomics study of flavivirus infection to examine the correlation of ISGs with intracellular viral RNA. To extend this arm of our analysis, we examined WNV-targeting antiviral effector genes that have been previously validated through short hairpin RNA (shRNA) and small interfering RNA (siRNA) knockdown screens, cell-based overexpression assays and *in vivo* knockout models (26, 42, 50-58). These validated antiviral effector genes exhibited both unimodal (*Tnfsf10*, *Ifi44l*, *Ifitm3*, *Eif2ak2* and *Mov10*) and bimodal (*Rsad2*, *Oas1b* and *Oas3*) expression patterns and all negatively correlated with viral RNA (Fig. 4, 6), demonstrating the technical capacity of WNV-inclusive scRNA-seq to probe virus-host interactions and identify novel antiviral candidate genes.

The discovery that bimodal variation in IFN-stimulated genes (ISGs) correlates with viral RNA abundance (Fig. 4, 6) bears notable relevance to previous work examining WNV antagonism of IFN-I signaling. WNV, among other flaviviruses, directly or indirectly antagonizes IFN-I signaling and the JAK-STAT pathway to counter cellular antiviral defenses (64-68). The WNV nonstructural protein NS5 blocks Jak1 and Tyk2 activation by interacting with prolidase to inhibit surface expression of IFNAR1 (10, 64). Additionally, WNV recruits plasma membrane-derived cholesterol to replication sites in the ER, and NS4A and NS4B contribute to membrane rearrangement and associated ER stress, which are all thought to interfere with JAK-STAT signaling (64, 69-71).

342 Bimodal ISG expression patterns correlated with viral abundance (Fig. 4, 6) may result
343 from viral antagonism in primary infected cells allowing for higher replication. This is
344 supported by the almost uniformly high expression observed for ISGs when limiting *in*
345 *vitro* spread (Fig. 4), a cell population with a predominantly low-level of WNV replication
346 (Fig. 2D). Alternatively, bimodality may arise from preexisting cell-intrinsic differences,
347 such as the level of critical signaling components, specifically at the initial stage of
348 infection.

349 WNV-inclusive scRNA-seq provides a single-cell transcriptomics protocol to
350 probe cellular heterogeneity in the host response and quantify viral RNA. The outlined
351 approach can potentially serve as a valuable tool for *in vivo* studies to examine cell-
352 intrinsic responses to viral infection, extending the resolution to infected single cells.
353 Such studies can also leverage the added ability with this approach to screen for
354 infected cells by qPCR and cherry pick cDNA for sequencing to mitigate cost. Our study
355 demonstrates the feasibility and utility of WNV-inclusive scRNA-seq as a high-
356 throughput technique for single-cell transcriptomics and viral RNA detection, which can
357 be used to provide insights into the cellular features of protective immunity.
358
359

MATERIALS AND METHODS

Cells and viruses. Murine fibroblast L929 cells were obtained from ATCC and grown at 37°C with 5% CO_2 in DMEM (Corning) supplemented with 10% heat-inactivated FBS, 2mM L-glutamine (Corning), 25 mM HEPES buffer (Corning), 1mM sodium pyruvate (Corning), MEM nonessential amino acids (Corning) and antibiotics/antimycotics (Corning). WNV isolate Texas 2002-HC (WNV-TX) has been previously described (3, 72, 73), and its titer was determined by standard plaque assay on BHK-21 cells. Working stocks were generated by passaging WNV-TX twice on Vero cells (ATCC CCL81) and used for *in vitro* experiments. WNV was incubated directly under ultraviolet (UV) light for 1 hr to generate UV-inactivated WNV, which was confirmed by plaque assay prior to use.

Infection and antibody treatment. L929 cells were plated to 70-80% confluent and infected with WNV-TX at different MOIs (0.1, 1 or 10). Following a 1 hr virus adsorption period at 37°C, cells were washed once with complete DMEM (cDMEM) and subsequently incubated for 6-48 hr with cDMEM or cDMEM supplemented with WNV E16 neutralizing antibody (5 μg/mL), a gift from Michael Diamond (Washington University, St. Louis, Missouri) (44). Cells were trypsinized for flow staining or lysed for RNA at 6, 12, 24 or 48 hr post-infection. Antibody titration in supplemental media was performed at multiple MOIs (0.1, 1 or 10) for 48 hr post-infection to determine the optimal concentration to considerably reduce *in vitro* spread prior to use.

382 **Flow cytometry.** Conditions were run in biological triplicate samples. Cells were treated
383 with 0.125% trypsin in PBS for 5 min at 37°C. All centrifugation steps were performed at
384 1250 rotations per minute for 5 min at 4°C. Cells were pelleted, resuspended in FACS
385 buffer (1x PBS, 1% FBS, 1 mM EDTA), and blocked for 10 min on ice with anti-mouse
386 Fc Shield (TONBO Biosciences) at 0.5 µL per sample in FACS buffer. Subsequently,
387 samples were stained for 20 min on ice with Ghost 780 viability dye (TONBO
388 Biosciences) at 0.1 µL per sample in PBS. Samples were washed and resuspended in
389 FACS buffer. For WNV E protein staining, samples were fixed following viability staining
390 with 1x Transcription Factor Fix/Perm (diluted in Transcription Factor Fix/Perm Diluent;
391 TONBO Biosciences) for 20 min on ice and washed twice with 1x Flow Cytometry Perm
392 Buffer (diluted in ddH_2O; TONBO Biosciences). WNV E16 antibody was conjugated to
393 Allophycocyanin (APC) using the Lightning-Link APC Antibody Labeling Kit (Novus
394 Biologicals). Samples were stained with APC-conjugated WNV E16 antibody at 0.25 µg
395 per sample in Flow Cytometry Perm Buffer for 30 min on ice. Samples were washed,
396 resuspended in FACS buffer, and run on a BD LSR II flow cytometer.
397
398 **Single-cell sorting.** Cells were stained with Ghost 780 viability dye (TONBO
399 Biosciences) as stated above and filtered through a 35 µm strainer into a 5 mL FACS
400 tube. Single viable cells were sorted into skirted 96-well PCR plates containing 10 µL
401 RLT buffer (Qiagen) with 2-betamercaptoethanol (1:100) per well using a BSL-3 level
402 BD Aria II flow cytometer.
403

Quantitative RT-PCR (qPCR). Time-matched mock and WNV-infected L929 cells (1×10^5 cells per condition; in triplicate) were lysed in RNA Lysis Buffer. Total RNA was isolated from cells using the Quick-RNA MiniPrep Kit (Zymo Research). Purified RNA was reverse transcribed using random primers with the High-Capacity cDNA Reverse Transcription Kit (Applied Biosystems). WNV RNA levels were quantified by qPCR using PrimeTime Gene Expression Master Mix (Integrated DNA Technologies), WNV-specific primers and probe set, and TaqMan gene expression assay (ThermoFisher) for the host gene *Gapdh* (Mm99999915_g1). WNV-specific primer and probe sequences (Forward primer: 5' – TCAGCGATCTCTCCACCAAAG – 3'; Reverse primer: 5' – GGGTCAGCACGTTTGTCATTG – 3'; and Probe: 5' – 6FAM-TGCCCGACC-ATGGGAGAAGCTC-MGB – 3') were adapted from Lanciotti and colleagues (73) and correspond to WNV isolate Texas 2002-HC (GenBank accession number: DQ176637.1). C_T values were normalized to the reference gene *Gapdh* and represented as fold change over time-matched mock values using the formula $2^{-\Delta\Delta CT}$. All primers and probes were purchased from Integrated DNA Technologies (IDT). qPCR was performed in 384-well plates and run on an Applied Biosystems 7900 HT Real-Time PCR System.

Bulk mRNA sequencing (RNA-seq). L929 cells were infected with WNV (MOI of 1) and incubated in the absence or presence (+Ab) of WNV E16 neutralizing Ab. In biological triplicate (n = 3), 50,000 viable cells were sorted into 100 µL RLT buffer (Qiagen) with 2-betamercaptoethanol (1:100) at 24 hr post-infection for each condition: time-matched mock, WNV and WNV (+Ab). mRNA sequencing libraries were prepared at Yerkes Genomics Core (http://www.yerkes.emory.edu/nhp_genomics_core/), and the

quality of the libraries was verified using DNA-1000 Kits (Agilent Bioanalyzer) and quantified using the Qubit 2.0 Fluorometer (LifeTechnologies). Libraries were clustered and sequenced on an Illumina HiSeq (100 bp single-end reads). Sequencing reads were mapped to the GENCODE mouse reference genome (GRCm38.p5 Release M16). Reads were normalized and differential expression analysis performed using DESeq2 (74). Normalized reads were expressed as fold change over time-matched mock values.

Single-cell RNA sequencing (scRNA-seq). SMART-Seq v4 Ultra Low Input RNA Kit (Takara) was used for cDNA preparation. The protocol was modified to include a WNV-specific viral primer during the RT step. WNV SC primer (5' – AAGCAGTGGTATCAACGCAGAGTACGGGTCAGCACGTTTGTCATTG – 3') targets the positive-sense envelope protein (E) gene (73) and contains the 5' 25-nucleotide ISPCR universal anchor sequence (underlined) from the Smart-seq2 protocol published by Picelli and colleagues (45) for downstream amplification alongside 3' SMART-Seq CDS Primer II A-primed transcripts. Similar to 3' SMART-Seq CDS Primer II A, 1 µL of WNV SC primer (12 µM) was added to the RT reaction for all samples. Other WNV-specific primer sequences and concentrations were evaluated. The scRNA-seq protocol was optimized to ensure high sensitivity for WNV RNA detection and to mitigate the formation of primer dimers or template-switching oligo (TSO) concatemers observed at high concentrations or with other primer sequences. During template switching, the RT product is extended with a sequence complementary to the TSO due to the addition of 2-5 untemplated nucleotides and the capacity of the RT enzyme to switch templates just as described in Smart-seq2 (45). PCR is performed using PCR Primer II A (the ISPCR

450 universal anchor sequence) for concurrent amplification of both host and viral cDNA.
451 Following PCR amplification, cDNA quantification is performed for each sample, and
452 cDNA quality assessment is accomplished using an Agilent 2100 Bioanalyzer. For
453 library preparation, amplified cDNA is fragmented and appended with dual-indexed
454 barcodes using Illumina Nextera XT DNA Library Prep kits. Sequencing was performed
455 using 101-bp single end reads at Yerkes Genomics Core
456 (http://www.yerkes.emory.edu/nhp_genomics_core/) as previously described (75) on an
457 Illumina HiSeq 3000 at a depth of ~1,000,000 reads per cell. In total, 127 cells were
458 successfully captured and profiled for single-cell transcriptomic analysis: 25 Mock cells,
459 68 WNV cells, and 34 WNV (+Ab) cells.
460
461 **Bioinformatics pipeline.** Libraries were sequenced on an Illumina HiSeq 3000
462 generating 101-bp single end reads. FastQC (76) was used to check the quality of fastq
463 files. The primary assembly of GENCODE mouse reference genome (GRCm38.p5
464 Release M16) (77) and the complete genome of WNV isolate Texas 2002-HC
465 (GenBank accession number: DQ176637.1) from ViPR (78) were used for mapping
466 reads. The genome index was built by combining both the genomes, and alignments
467 were carried out for the combined genomes. STAR v2.5.2b (79) was used with default
468 parameters to map reads and obtain reads per gene counts (–quantMode Gene
469 Counts). The counts obtained with STAR were used for downstream analysis in R. The
470 counts were used to create a SingleCellExperiment v1.0.0 (80) object. The scater v1.6.3
471 (81) library was used for quality control of cells. Genes that were not expressed in any
472 cell were filtered out. The isOutlier function from scran was used to remove cells that

had a library size and number of detected genes greater than 3 median absolute deviations lower than the median values or those with percentage of mitochondrial genes that were 3 median absolute deviations higher than the median value (82). The cell cycle phase was predicted using the cyclone function in scran package v1.6.3 (80, 82). The normalized expression values were obtained using the calculateCPM function in the scater library.

Statistical analysis and software. Prism 6 (GraphPad), ggplot2 R package, ggridges R package, corrplot R package and Hmisc R package were used for statistical analyses and graphical presentation of data. Spearman's rank correlation coefficients (ρ) and associated *p* values were computed for each gene pairing using the rcorr function in Hmisc R package. Two-way ANOVA with Tukey's multiple comparison correction was used to evaluate significant differences between conditions for percentage of WNV E-positive cells and relative viral RNA. Wilcoxon rank-sum test with continuity correction was performed to assess significant differences between single-cell distributions for host mRNA and viral RNA counts per million transcripts (CPM).

FIGURE LEGENDS

Figure 1. Population-level analysis of WNV infection in L929 cells.

(A) L929 cells were infected with WNV at a MOI of 0.1, 1, or 10 and incubated for 6, 12, 24, or 48 hr (n = 3). (A-B) Intracellular viral E protein staining was performed by flow cytometry using WNV E16 antibody. (B-C) L929 cells were inoculated with UV-inactivated WNV (UV) or WNV at a MOI of 1 and incubated for 12 or 24 hr in the presence (+Ab) or absence of WNV E16 neutralizing antibody (5 μg/mL) to reduce *in vitro* spread (n = 3). (C) Viral RNA quantification was measured by qPCR, and C_T values were normalized to the reference gene *Gapdh* and represented as fold change over time-matched mock values. (A-C) Two-way ANOVA with multiple comparison correction was used to test for significance (*$p < 0.05$). (D-F) Cells were infected as in (B) and examined by bulk RNA-seq analysis at 24 hr post-infection (n = 3). (D-E) Heat map showing mean gene expression values normalized and represented as fold change over time-matched mock values. Expression fold change values correspond to the color gradient (bottom). (D) Gene cluster description can be found on the left. (E) Expression fold change displayed for a panel of select genes. (F) Scatter plot for comparison of up-regulated and down-regulated genes in WNV and WNV (+Ab) conditions. Cut-off values were as follows: 1.5 fold change and $p < 0.01$.

Figure 2. WNV-inclusive single-cell RNA sequencing.

(A) L929 cells were infected with WNV (MOI of 1) and incubated in the presence of the WNV E16 neutralizing Ab (5 μg/mL) to limit *in vitro* spread. (B) Single cells were sorted into 96-well PCR plates containing 10 μL lysis buffer per well. (C) During reverse

515 transcription (RT), 3' SMART-Seq CDS Primer II A (30-nucleotide poly-dT sequence
516 with a 5' 25-nucleotide ISPCR universal anchor sequence) and a WNV-specific viral
517 primer (21-nucleotide sequence complementary to positive-strand viral RNA with a 5'
518 25-nucleotide ISPCR universal anchor sequence) are added to capture host transcripts
519 and viral RNA, respectively. When the reverse transcriptase reaches the 5' end of both
520 host mRNA and viral RNA, its terminal transferase activity adds 2-5 untemplated
521 nucleotides that serve as an anchor for the template-switching oligo (TSO), which
522 allows extension of the RT product with sequence complementary to the universal
523 anchor sequence. PCR Primer II A binds this sequence for concurrent amplification of
524 both host and viral cDNA. In the final library preparation step, transposase 5 (Tn5)-
525 based Nextera tagmentation adds sequencing indexes. Illumina sequencing is
526 performed using 101-bp single end reads, thereby quantifying host mRNA and viral
527 RNA from single cells. (B-C) In total, 127 cells were successfully captured and profiled:
528 25 Mock cells, 68 WNV cells, and 34 WNV (+Ab) cells. (D) Coverage and alignment of
529 WNV reads are shown with reference to the WNV genome and WNV SC primer (viral
530 primer) location, and y-axes are in log10 scale. The cells representing the median value
531 for WNV and Mock conditions are shown. Violin plot showing expression as counts per
532 million transcripts (CPM) in log2 scale for WNV RNA in all three conditions described in
533 2A. Wilcoxon rank-sum test with continuity correction was performed to test significance
534 (**$p < 10^{-9}$). (E) Violin plots showing expression as CPM in log2 scale for housekeeping
535 genes. Wilcoxon rank-sum test with continuity correction was performed to test
536 significance (ns = not significant; *$p < 10^{-3}$; **$p < 10^{-6}$).
537

538 **Figure 3. Cellular heterogeneity in IFN-stimulated gene induction following WNV**
539 **infection.**
540 Violin plots showing single-cell distributions for host gene expression as counts per
541 million transcripts (CPM) in log2 scale. Genes are grouped by categories: (A) IFN-I
542 production and other cytokines; and (B) PRR and IFN-I signaling. Conditions are
543 described in Fig. 2A. Wilcoxon rank-sum test with continuity correction was performed
544 to test significance (ns = not significant; *$p < 10^{-3}$; **$p < 10^{-6}$).
545
546 **Figure 4. Unimodal and bimodal variation in antiviral effector gene expression at**
547 **single-cell following WNV infection.**
548 Violin plots showing single-cell distributions for antiviral effector gene expression as
549 counts per million transcripts (CPM) in log2 scale. Conditions are described in Fig. 2A.
550 Wilcoxon rank-sum test with continuity correction was performed to test significance (ns
551 = not significant; *$p < 10^{-3}$; **$p < 10^{-6}$).
552
553 **Figure 5. ISGs negatively correlate with WNV RNA abundance.**
554 (A) Gene ontology (GO) enrichment analysis for genes significantly ($p < 0.001$)
555 positively correlated ($\rho > 0.35$) and negatively correlated ($\rho < -0.35$) with viral RNA.
556 Enrichment scores (ES) calculated for each pathway by the formula: $-\log_{10}(p \text{ value})$.
557 Dotted line indicates significance cutoff ($p = 0.05$; ES = 1.3). (B) Density plots of host
558 gene expression correlated viral RNA across all WNV cells. Spearman's correlation
559 coefficients (ρ) calculated for each host gene by viral RNA. Gene set labels (left) and
560 totals (right) are shown. Cell cycle-associated genes are additionally subdivided by

phase. Select genes were marked and labeled. Dotted lines indicate correlation coefficients (ρ) equal to -0.35 and 0.35. (C) Correlation matrix for 57 of 124 negatively correlated ISGs, all positively correlated ISGs, 9 non-correlated cytokine genes and WNV RNA. Correlation coefficients (ρ) calculated for each gene pairing are indicated by the color gradient (bottom). White boxes represent comparisons for which the correlation did not meet the significance cutoff ($p < 0.001$).

Figure 6. Sharp downward trend for ISGs negatively correlated with viral RNA. Scatter plots showing expression as counts per million transcripts (CPM) in log2 scale of positively and negatively correlated host genes by WNV RNA. Each cell is represented by a single dot with minimal transparency so areas of high density are easily discernable. Correlation coefficients (ρ) are indicated for each gene and correspond to the color gradient (top). Scatter plots have been collated from lowest to highest correlation coefficient. All genes shown here meet the following criteria: $|\rho| > 0.4$ and $p < 0.0005$.

578 **Acknowledgments**

579 We thank the Emory Vaccine Center Flow Core, specifically Kiran Gill and Barbara
580 Cervasi, for assistance with cell sorting and the Yerkes Genomics Core for library
581 preparation and sequencing.

582

583

Funding Information

This work was funded in part by National Institutes of Health grants U19AI083019 (M.S.S), (M.S.S), 5U19AI106772 (M.S.S), R21AI113485 (M.S.S.), ORIP/OD P51OD011132 (M.S.S), Emory University Department of Pediatrics Junior Faculty Focused Award (M.S.S), Children's Healthcare of Atlanta, Emory Vaccine Center, and The Georgia Research Alliance (M.S.S). The funders had no role in study design, data collection and analysis, decision to publish, or preparation of the manuscript.

BIBLIOGRAPHY

1. Chancey C, Grinev A, Volkova E, Rios M. 2015. The global ecology and epidemiology of West Nile virus. Biomed Res Int 2015:376230.
2. Krow-Lucal E, Lindsey NP, Lehman J, Fischer M, Staples JE. 2017. West Nile Virus and Other Nationally Notifiable Arboviral Diseases - United States, 2015. MMWR Morb Mortal Wkly Rep 66:51-55.
3. Suthar MS, Diamond MS, Gale M, Jr. 2013. West Nile virus infection and immunity. Nat Rev Microbiol 11:115-28.
4. Swanson PA, 2nd, McGavern DB. 2015. Viral diseases of the central nervous system. Curr Opin Virol 11:44-54.
5. Brien JD, Uhrlaub JL, Nikolich-Zugich J. 2008. West Nile virus-specific CD4 T cells exhibit direct antiviral cytokine secretion and cytotoxicity and are sufficient for antiviral protection. J Immunol 181:8568-75.
6. Durrant DM, Robinette ML, Klein RS. 2013. IL-1R1 is required for dendritic cell-mediated T cell reactivation within the CNS during West Nile virus encephalitis. J Exp Med 210:503-16.
7. Gorman MJ, Caine EA, Zaitsev K, Begley MC, Weger-Lucarelli J, Uccellini MB, Tripathi S, Morrison J, Yount BL, Dinnon KH, 3rd, Ruckert C, Young MC, Zhu Z, Robertson SJ, McNally KL, Ye J, Cao B, Mysorekar IU, Ebel GD, Baric RS, Best SM, Artyomov MN, Garcia-Sastre A, Diamond MS. 2018. An Immunocompetent Mouse Model of Zika Virus Infection. Cell Host Microbe 23:672-685 e6.
8. Klein RS, Lin E, Zhang B, Luster AD, Tollett J, Samuel MA, Engle M, Diamond MS. 2005. Neuronal CXCL10 directs CD8+ T-cell recruitment and control of West Nile virus encephalitis. J Virol 79:11457-66.

9. Lazear HM, Lancaster A, Wilkins C, Suthar MS, Huang A, Vick SC, Clepper L, Thackray L, Brassil MM, Virgin HW, Nikolich-Zugich J, Moses AV, Gale M, Jr., Fruh K, Diamond MS. 2013. IRF-3, IRF-5, and IRF-7 coordinately regulate the type I IFN response in myeloid dendritic cells downstream of MAVS signaling. PLoS Pathog 9:e1003118.

10. Lubick KJ, Robertson SJ, McNally KL, Freedman BA, Rasmussen AL, Taylor RT, Walts AD, Tsuruda S, Sakai M, Ishizuka M, Boer EF, Foster EC, Chiramel AI, Addison CB, Green R, Kastner DL, Katze MG, Holland SM, Forlino A, Freeman AF, Boehm M, Yoshii K, Best SM. 2015. Flavivirus Antagonism of Type I Interferon Signaling Reveals Prolidase as a Regulator of IFNAR1 Surface Expression. Cell Host Microbe 18:61-74.

11. Pinto AK, Ramos HJ, Wu X, Aggarwal S, Shrestha B, Gorman M, Kim KY, Suthar MS, Atkinson JP, Gale M, Jr., Diamond MS. 2014. Deficient IFN signaling by myeloid cells leads to MAVS-dependent virus-induced sepsis. PLoS Pathog 10:e1004086.

12. Schneider WM, Chevillotte MD, Rice CM. 2014. Interferon-stimulated genes: a complex web of host defenses. Annu Rev Immunol 32:513-45.

13. Sen A, Rothenberg ME, Mukherjee G, Feng N, Kalisky T, Nair N, Johnstone IM, Clarke MF, Greenberg HB. 2012. Innate immune response to homologous rotavirus infection in the small intestinal villous epithelium at single-cell resolution. Proc Natl Acad Sci U S A 109:20667-72.

14. Suthar MS, Ma DY, Thomas S, Lund JM, Zhang N, Daffis S, Rudensky AY, Bevan MJ, Clark EA, Kaja MK, Diamond MS, Gale M, Jr. 2010. IPS-1 is essential

for the control of West Nile virus infection and immunity. PLoS Pathog 6:e1000757.

15. Samuel MA, Diamond MS. 2005. Alpha/beta interferon protects against lethal West Nile virus infection by restricting cellular tropism and enhancing neuronal survival. J Virol 79:13350-61.

16. Hu J, Nudelman G, Shimoni Y, Kumar M, Ding Y, Lopez C, Hayot F, Wetmur JG, Sealfon SC. 2011. Role of cell-to-cell variability in activating a positive feedback antiviral response in human dendritic cells. PLoS One 6:e16614.

17. Patil S, Fribourg M, Ge Y, Batish M, Tyagi S, Hayot F, Sealfon SC. 2015. Single-cell analysis shows that paracrine signaling by first responder cells shapes the interferon-beta response to viral infection. Sci Signal 8:ra16.

18. Rand U, Rinas M, Schwerk J, Nohren G, Linnes M, Kroger A, Flossdorf M, Kaly-Kullai K, Hauser H, Hofer T, Koster M. 2012. Multi-layered stochasticity and paracrine signal propagation shape the type-I interferon response. Mol Syst Biol 8:584.

19. Zhao M, Zhang J, Phatnani H, Scheu S, Maniatis T. 2012. Stochastic expression of the interferon-beta gene. PLoS Biol 10:e1001249.

20. Sadler AJ, Williams BR. 2008. Interferon-inducible antiviral effectors. Nat Rev Immunol 8:559-68.

21. Schoggins JW. 2014. Interferon-stimulated genes: roles in viral pathogenesis. Curr Opin Virol 6:40-6.

661 22. Honda K, Takaoka A, Taniguchi T. 2006. Type I interferon [corrected] gene
662 induction by the interferon regulatory factor family of transcription factors.
663 Immunity 25:349-60.
664 23. Ashour J, Laurent-Rolle M, Shi PY, Garcia-Sastre A. 2009. NS5 of dengue virus
665 mediates STAT2 binding and degradation. J Virol 83:5408-18.
666 24. Grant A, Ponia SS, Tripathi S, Balasubramaniam V, Miorin L, Sourisseau M,
667 Schwarz MC, Sanchez-Seco MP, Evans MJ, Best SM, Garcia-Sastre A. 2016.
668 Zika Virus Targets Human STAT2 to Inhibit Type I Interferon Signaling. Cell Host
669 Microbe 19:882-90.
670 25. Morrison J, Laurent-Rolle M, Maestre AM, Rajsbaum R, Pisanelli G, Simon V,
671 Mulder LC, Fernandez-Sesma A, Garcia-Sastre A. 2013. Dengue virus co-opts
672 UBR4 to degrade STAT2 and antagonize type I interferon signaling. PLoS
673 Pathog 9:e1003265.
674 26. Schoggins JW, Wilson SJ, Panis M, Murphy MY, Jones CT, Bieniasz P, Rice CM.
675 2011. A diverse range of gene products are effectors of the type I interferon
676 antiviral response. Nature 472:481-5.
677 27. Shalek AK, Satija R, Shuga J, Trombetta JJ, Gennert D, Lu D, Chen P, Gertner
678 RS, Gaublomme JT, Yosef N, Schwartz S, Fowler B, Weaver S, Wang J, Wang
679 X, Ding R, Raychowdhury R, Friedman N, Hacohen N, Park H, May AP, Regev A.
680 2014. Single-cell RNA-seq reveals dynamic paracrine control of cellular variation.
681 Nature 510:363-9.
682 28. Daffis S, Szretter KJ, Schriewer J, Li J, Youn S, Errett J, Lin TY, Schneller S,
683 Zust R, Dong H, Thiel V, Sen GC, Fensterl V, Klimstra WB, Pierson TC, Buller

RM, Gale M, Jr., Shi PY, Diamond MS. 2010. 2'-O methylation of the viral mRNA cap evades host restriction by IFIT family members. Nature 468:452-6.

29. Russell AB, Trapnell C, Bloom JD. 2018. Extreme heterogeneity of influenza virus infection in single cells. Elife 7.

30. Schulte MB, Andino R. 2014. Single-cell analysis uncovers extensive biological noise in poliovirus replication. J Virol 88:6205-12.

31. Zanini F, Pu SY, Bekerman E, Einav S, Quake SR. 2018. Single-cell transcriptional dynamics of flavivirus infection. Elife 7.

32. Hamlin RE, Rahman A, Pak TR, Maringer K, Mena I, Bernal-Rubio D, Potla U, Maestre AM, Fredericks AC, Amir ED, Kasarskis A, Ramos I, Merad M, Fernandez-Sesma A. 2017. High-dimensional CyTOF analysis of dengue virus-infected human DCs reveals distinct viral signatures. JCI Insight 2.

33. Avraham R, Haseley N, Brown D, Penaranda C, Jijon HB, Trombetta JJ, Satija R, Shalek AK, Xavier RJ, Regev A, Hung DT. 2015. Pathogen Cell-to-Cell Variability Drives Heterogeneity in Host Immune Responses. Cell 162:1309-21.

34. Alvarez-Errico D, Vento-Tormo R, Sieweke M, Ballestar E. 2015. Epigenetic control of myeloid cell differentiation, identity and function. Nat Rev Immunol 15:7-17.

35. Ford E, Thanos D. 2010. The transcriptional code of human IFN-beta gene expression. Biochim Biophys Acta 1799:328-36.

36. Xue S, Liu C, Sun X, Li W, Zhang C, Zhou X, Lu Y, Xiao J, Li C, Xu X, Sun B, Xu G, Wang H. 2016. TET3 Inhibits Type I IFN Production Independent of DNA Demethylation. Cell Rep 16:1096-1105.

37. Kwon YJ, Heo J, Wong HE, Cruz DJ, Velumani S, da Silva CT, Mosimann AL, Duarte Dos Santos CN, Freitas-Junior LH, Fink K. 2014. Kinome siRNA screen identifies novel cell-type specific dengue host target genes. Antiviral Res 110:20-30.

38. Marceau CD, Puschnik AS, Majzoub K, Ooi YS, Brewer SM, Fuchs G, Swaminathan K, Mata MA, Elias JE, Sarnow P, Carette JE. 2016. Genetic dissection of Flaviviridae host factors through genome-scale CRISPR screens. Nature 535:159-63.

39. Zhang R, Miner JJ, Gorman MJ, Rausch K, Ramage H, White JP, Zuiani A, Zhang P, Fernandez E, Zhang Q, Dowd KA, Pierson TC, Cherry S, Diamond MS. 2016. A CRISPR screen defines a signal peptide processing pathway required by flaviviruses. Nature 535:164-8.

40. Krishnan MN, Ng A, Sukumaran B, Gilfoy FD, Uchil PD, Sultana H, Brass AL, Adametz R, Tsui M, Qian F, Montgomery RR, Lev S, Mason PW, Koski RA, Elledge SJ, Xavier RJ, Agaisse H, Fikrig E. 2008. RNA interference screen for human genes associated with West Nile virus infection. Nature 455:242-5.

41. Ma H, Dang Y, Wu Y, Jia G, Anaya E, Zhang J, Abraham S, Choi JG, Shi G, Qi L, Manjunath N, Wu H. 2015. A CRISPR-Based Screen Identifies Genes Essential for West-Nile-Virus-Induced Cell Death. Cell Rep 12:673-83.

42. Li J, Ding SC, Cho H, Chung BC, Gale M, Jr., Chanda SK, Diamond MS. 2013. A short hairpin RNA screen of interferon-stimulated genes identifies a novel negative regulator of the cellular antiviral response. MBio 4:e00385-13.

729 43. Hoss-Homfeld A, Zwarthoff EC, Zawatzky R. 1989. Cell type specific expression
730 and regulation of murine interferon alpha and beta genes. Virology 173:539-50.
731 44. Nybakken GE, Oliphant T, Johnson S, Burke S, Diamond MS, Fremont DH. 2005.
732 Structural basis of West Nile virus neutralization by a therapeutic antibody.
733 Nature 437:764-9.
734 45. Picelli S, Faridani OR, Bjorklund AK, Winberg G, Sagasser S, Sandberg R. 2014.
735 Full-length RNA-seq from single cells using Smart-seq2. Nat Protoc 9:171-81.
736 46. Wu AR, Neff NF, Kalisky T, Dalerba P, Treutlein B, Rothenberg ME, Mburu FM,
737 Mantalas GL, Sim S, Clarke MF, Quake SR. 2014. Quantitative assessment of
738 single-cell RNA-sequencing methods. Nat Methods 11:41-6.
739 47. Marie I, Durbin JE, Levy DE. 1998. Differential viral induction of distinct
740 interferon-alpha genes by positive feedback through interferon regulatory factor-7.
741 EMBO J 17:6660-9.
742 48. Sato M, Hata N, Asagiri M, Nakaya T, Taniguchi T, Tanaka N. 1998. Positive
743 feedback regulation of type I IFN genes by the IFN-inducible transcription factor
744 IRF-7. FEBS Lett 441:106-10.
745 49. Sato M, Suemori H, Hata N, Asagiri M, Ogasawara K, Nakao K, Nakaya T,
746 Katsuki M, Noguchi S, Tanaka N, Taniguchi T. 2000. Distinct and essential roles
747 of transcription factors IRF-3 and IRF-7 in response to viruses for IFN-alpha/beta
748 gene induction. Immunity 13:539-48.
749 50. Brass AL, Huang IC, Benita Y, John SP, Krishnan MN, Feeley EM, Ryan BJ,
750 Weyer JL, van der Weyden L, Fikrig E, Adams DJ, Xavier RJ, Farzan M, Elledge

751 SJ. 2009. The IFITM proteins mediate cellular resistance to influenza A H1N1
752 virus, West Nile virus, and dengue virus. Cell 139:1243-54.
753 51. Gorman MJ, Poddar S, Farzan M, Diamond MS. 2016. The Interferon-Stimulated
754 Gene Ifitm3 Restricts West Nile Virus Infection and Pathogenesis. J Virol
755 90:8212-25.
756 52. Kajaste-Rudnitski A, Mashimo T, Frenkiel MP, Guenet JL, Lucas M, Despres P.
757 2006. The 2',5'-oligoadenylate synthetase 1b is a potent inhibitor of West Nile
758 virus replication inside infected cells. J Biol Chem 281:4624-37.
759 53. Liu XY, Chen W, Wei B, Shan YF, Wang C. 2011. IFN-induced TPR protein IFIT3
760 potentiates antiviral signaling by bridging MAVS and TBK1. J Immunol 187:2559-
761 68.
762 54. Perelygin AA, Scherbik SV, Zhulin IB, Stockman BM, Li Y, Brinton MA. 2002.
763 Positional cloning of the murine flavivirus resistance gene. Proc Natl Acad Sci U
764 S A 99:9322-7.
765 55. Szretter KJ, Brien JD, Thackray LB, Virgin HW, Cresswell P, Diamond MS. 2011.
766 The interferon-inducible gene viperin restricts West Nile virus pathogenesis. J
767 Virol 85:11557-66.
768 56. Verhelst J, Parthoens E, Schepens B, Fiers W, Saelens X. 2012. Interferon-
769 inducible protein Mx1 inhibits influenza virus by interfering with functional viral
770 ribonucleoprotein complex assembly. J Virol 86:13445-55.
771 57. Shrestha B, Pinto AK, Green S, Bosch I, Diamond MS. 2012. CD8+ T cells use
772 TRAIL to restrict West Nile virus pathogenesis by controlling infection in neurons.
773 J Virol 86:8937-48.

774 58. Li Y, Banerjee S, Wang Y, Goldstein SA, Dong B, Gaughan C, Silverman RH,
775 Weiss SR. 2016. Activation of RNase L is dependent on OAS3 expression during
776 infection with diverse human viruses. Proc Natl Acad Sci U S A 113:2241-6.
777 59. Huang da W, Sherman BT, Lempicki RA. 2009. Systematic and integrative
778 analysis of large gene lists using DAVID bioinformatics resources. Nat Protoc
779 4:44-57.
780 60. Huang da W, Sherman BT, Lempicki RA. 2009. Bioinformatics enrichment tools:
781 paths toward the comprehensive functional analysis of large gene lists. Nucleic
782 Acids Res 37:1-13.
783 61. Macosko EZ, Basu A, Satija R, Nemesh J, Shekhar K, Goldman M, Tirosh I,
784 Bialas AR, Kamitaki N, Martersteck EM, Trombetta JJ, Weitz DA, Sanes JR,
785 Shalek AK, Regev A, McCarroll SA. 2015. Highly Parallel Genome-wide
786 Expression Profiling of Individual Cells Using Nanoliter Droplets. Cell 161:1202-
787 1214.
788 62. Baranek T, Manh TP, Alexandre Y, Maqbool MA, Cabeza JZ, Tomasello E,
789 Crozat K, Bessou G, Zucchini N, Robbins SH, Vivier E, Kalinke U, Ferrier P,
790 Dalod M. 2012. Differential responses of immune cells to type I interferon
791 contribute to host resistance to viral infection. Cell Host Microbe 12:571-84.
792 63. Illumina Inc. 2017. Effects of Index Misassignment on Multiplexing and
793 Downstream Analysis.
794 64. Best SM. 2017. The Many Faces of the Flavivirus NS5 Protein in Antagonism of
795 Type I Interferon Signaling. J Virol 91.

796 65. Bowen JR, Zimmerman MG, Suthar MS. 2017. Taking the defensive: Immune
797 control of Zika virus infection. Virus Res doi:10.1016/j.virusres.2017.08.018.
798 66. Quicke KM, Diamond MS, Suthar MS. 2017. Negative regulators of the RIG-I-like
799 receptor signaling pathway. Eur J Immunol 47:615-628.
800 67. Quicke KM, Suthar MS. 2013. The innate immune playbook for restricting West
801 Nile virus infection. Viruses 5:2643-58.
802 68. Bowen JR, Quicke KM, Maddur MS, O'Neal JT, McDonald CE, Fedorova NB,
803 Puri V, Shabman RS, Pulendran B, Suthar MS. 2017. Zika Virus Antagonizes
804 Type I Interferon Responses during Infection of Human Dendritic Cells. PLoS
805 Pathog 13:e1006164.
806 69. Ambrose RL, Mackenzie JM. 2011. West Nile virus differentially modulates the
807 unfolded protein response to facilitate replication and immune evasion. J Virol
808 85:2723-32.
809 70. Mackenzie JM, Khromykh AA, Parton RG. 2007. Cholesterol manipulation by
810 West Nile virus perturbs the cellular immune response. Cell Host Microbe 2:229-
811 39.
812 71. Roosendaal J, Westaway EG, Khromykh A, Mackenzie JM. 2006. Regulated
813 cleavages at the West Nile virus NS4A-2K-NS4B junctions play a major role in
814 rearranging cytoplasmic membranes and Golgi trafficking of the NS4A protein. J
815 Virol 80:4623-32.
816 72. Aguilar-Valenzuela R, Netland J, Seo YJ, Bevan MJ, Grakoui A, Suthar MS.
817 2018. Dynamics of Tissue-Specific CD8(+) T Cell Responses during West Nile
818 Virus Infection. J Virol 92.

819 73. Lanciotti RS, Kerst AJ, Nasci RS, Godsey MS, Mitchell CJ, Savage HM, Komar N,
820 Panella NA, Allen BC, Volpe KE, Davis BS, Roehrig JT. 2000. Rapid detection of
821 west nile virus from human clinical specimens, field-collected mosquitoes, and
822 avian samples by a TaqMan reverse transcriptase-PCR assay. J Clin Microbiol
823 38:4066-71.
824 74. Love MI, Huber W, Anders S. 2014. Moderated estimation of fold change and
825 dispersion for RNA-seq data with DESeq2. Genome Biol 15:550.
826 75. Upadhyay AA, Kauffman RC, Wolabaugh AN, Cho A, Patel NB, Reiss SM,
827 Havenar-Daughton C, Dawoud RA, Tharp GK, Sanz I, Pulendran B, Crotty S,
828 Lee FE, Wrammert J, Bosinger SE. 2018. BALDR: a computational pipeline for
829 paired heavy and light chain immunoglobulin reconstruction in single-cell RNA-
830 seq data. Genome Med 10:20.
831 76. Andrews S. 2010. FastQC: a quality control tool for high throughput sequence
832 data,
833 77. Harrow J, Frankish A, Gonzalez JM, Tapanari E, Diekhans M, Kokocinski F,
834 Aken BL, Barrell D, Zadissa A, Searle S, Barnes I, Bignell A, Boychenko V, Hunt
835 T, Kay M, Mukherjee G, Rajan J, Despacio-Reyes G, Saunders G, Steward C,
836 Harte R, Lin M, Howald C, Tanzer A, Derrien T, Chrast J, Walters N,
837 Balasubramanian S, Pei B, Tress M, Rodriguez JM, Ezkurdia I, van Baren J,
838 Brent M, Haussler D, Kellis M, Valencia A, Reymond A, Gerstein M, Guigo R,
839 Hubbard TJ. 2012. GENCODE: the reference human genome annotation for The
840 ENCODE Project. Genome Res 22:1760-74.

78. Pickett BE, Sadat EL, Zhang Y, Noronha JM, Squires RB, Hunt V, Liu M, Kumar S, Zaremba S, Gu Z, Zhou L, Larson CN, Dietrich J, Klem EB, Scheuermann RH. 2012. ViPR: an open bioinformatics database and analysis resource for virology research. Nucleic Acids Res 40:D593-8.

79. Dobin A, Davis CA, Schlesinger F, Drenkow J, Zaleski C, Jha S, Batut P, Chaisson M, Gingeras TR. 2013. STAR: ultrafast universal RNA-seq aligner. Bioinformatics 29:15-21.

80. Lun AR, D. 2018. Single Cell Experiment: S4 Classes for Single Cell Data, Bioconductor.

81. McCarthy DJ, Campbell KR, Lun AT, Wills QF. 2017. Scater: pre-processing, quality control, normalization and visualization of single-cell RNA-seq data in R. Bioinformatics 33:1179-1186.

82. Scialdone A, Natarajan KN, Saraiva LR, Proserpio V, Teichmann SA, Stegle O, Marioni JC, Buettner F. 2015. Computational assignment of cell-cycle stage from single-cell transcriptome data. Methods 85:54-61.

Figure 1

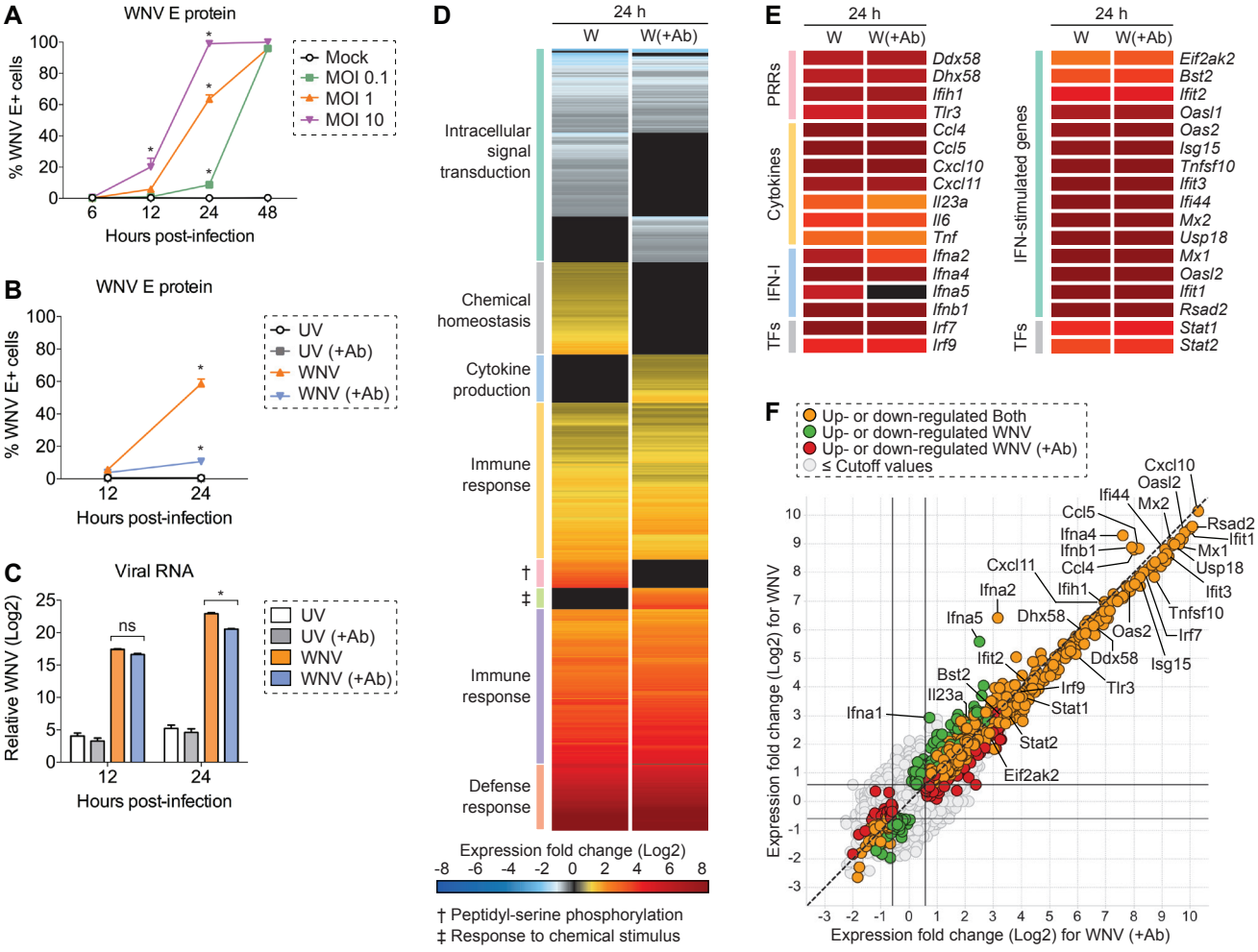

Figure 2

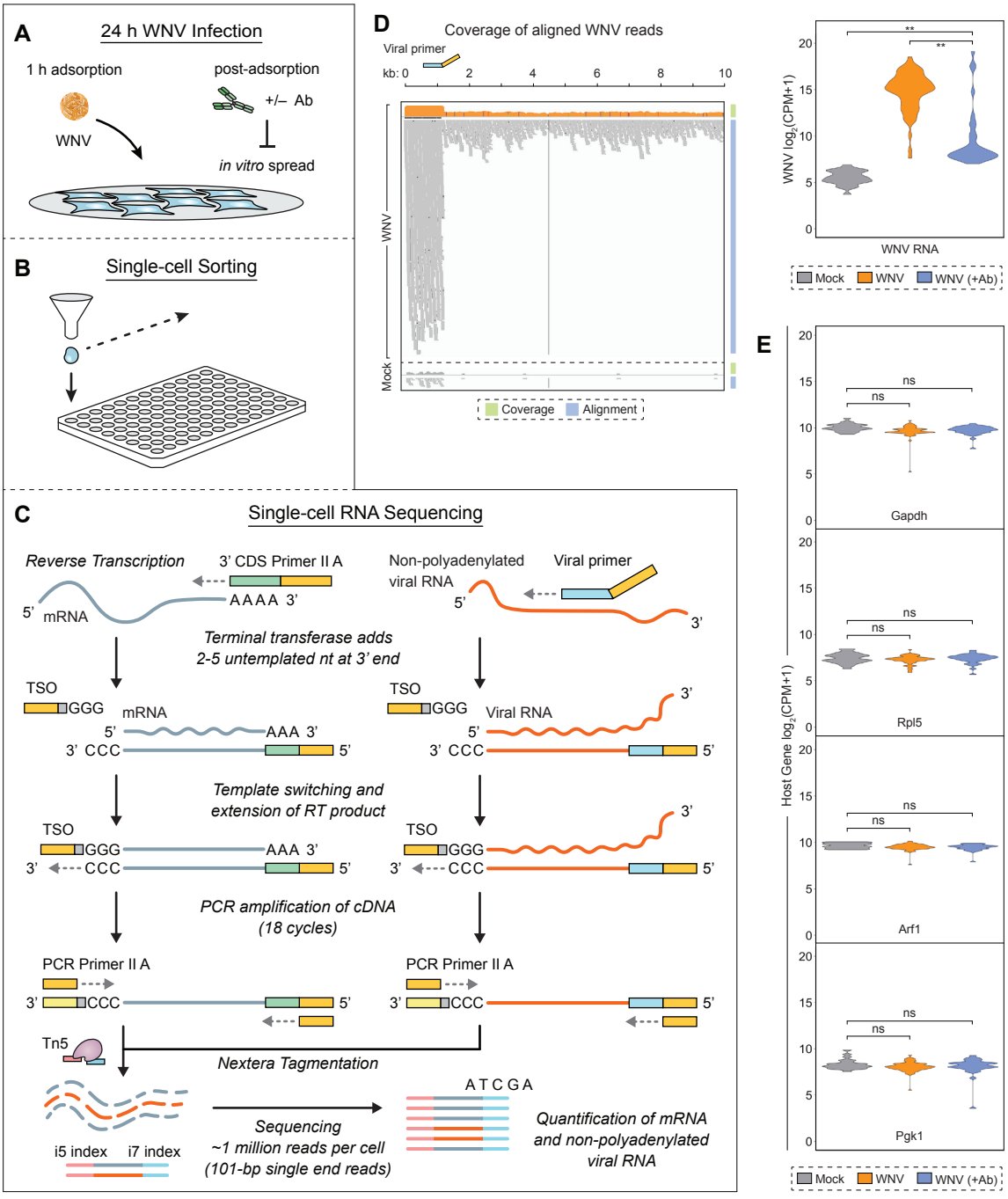

Figure 3

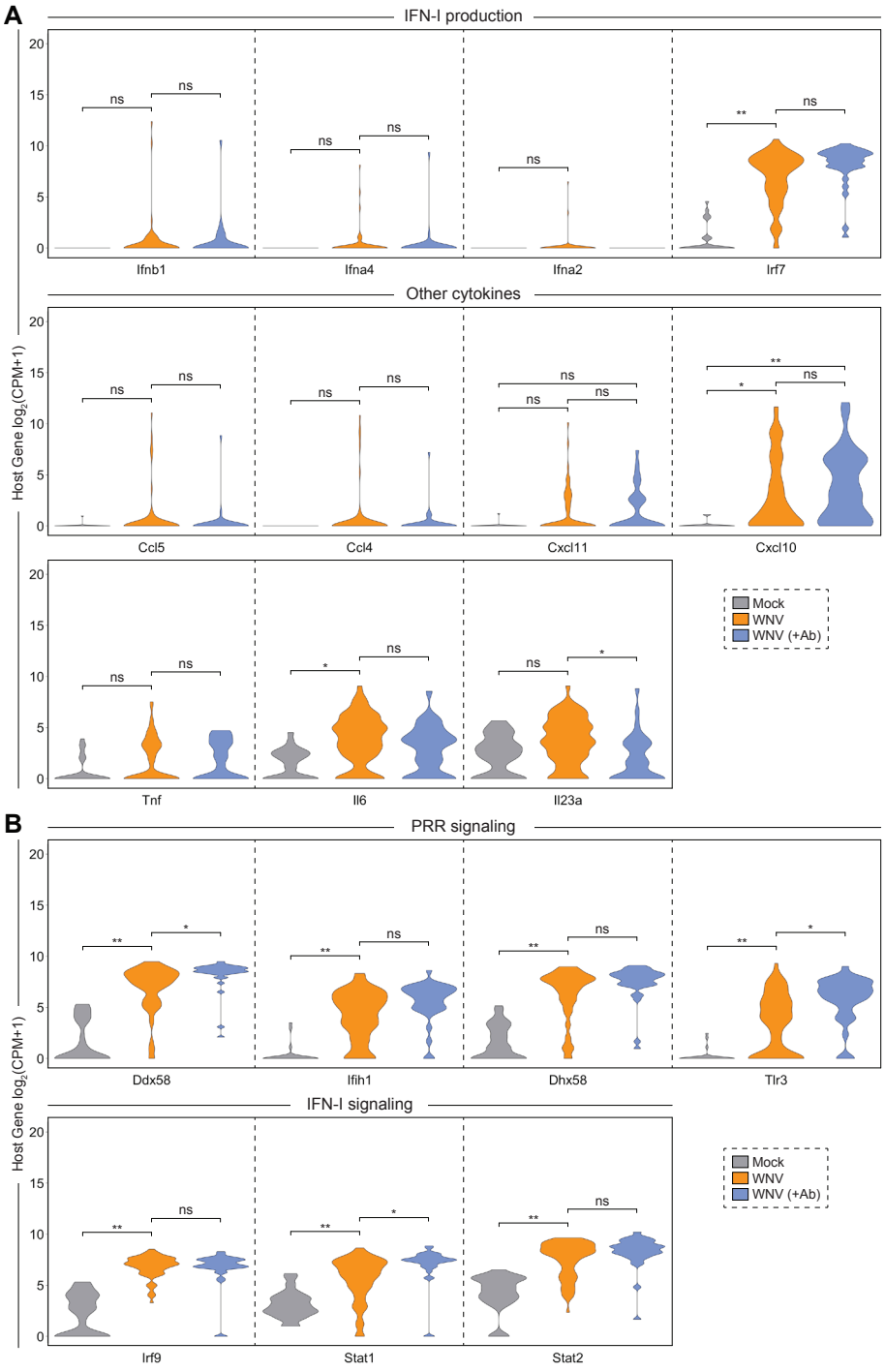

Figure 4

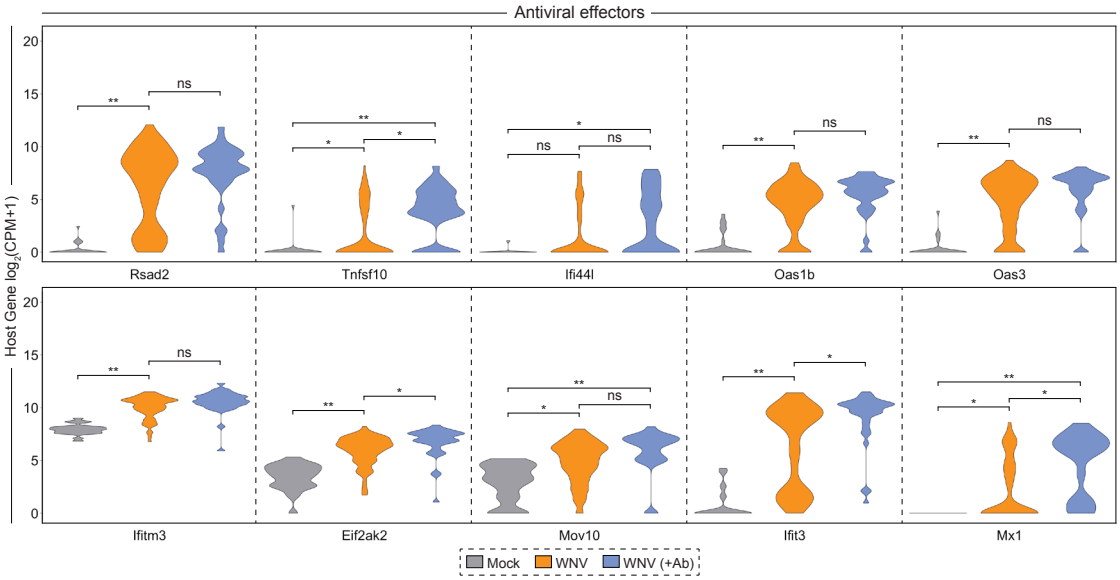

Figure 5

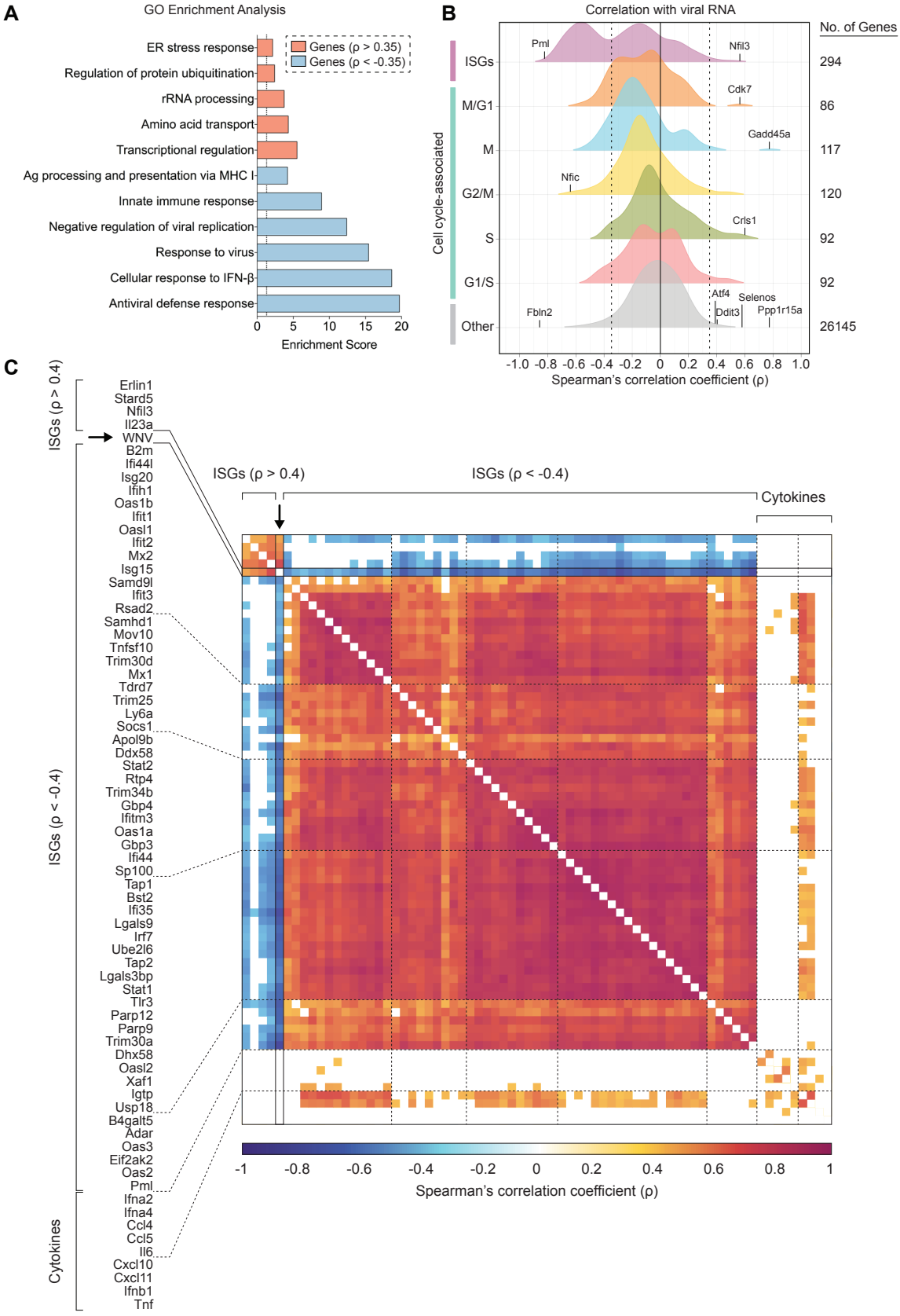

Figure 6